JOURNAL OF Materials CHEMISTRY

Study of the formation of mesoporous titania *via* a template approach and of subsequent Li insertion†

Fabrice Leroux,[a] Patricia J. Dewar,[b] Mourad Intissar,[a] Guy Ouvrard*[c] and Linda F. Nazar[b]

[a]*Laboratoire des Matériaux Inorganiques, CNRS UPRES-A 6002, Université Blaise Pascal, 63177 Aubière cédex, France*
[b]*Department of Chemistry, University of Waterloo, Waterloo N2L 3G1, Ontario, Canada. E-mail: lfnazar@uwaterloo.ca*
[c]*Institut des Matériaux Jean Rouxel, Ecole Polytechnique de l'Université de Nantes, CNRS UMR 6502, 2 rue de la Houssinière, BP 32229, 44322 Nantes cédex 03, France. E-mail: ouvrard@cnrs-imn.fr*

Received 26th April 2002, Accepted 23rd July 2002
First published as an Advance Article on the web 3rd October 2002

Mesostructured titania was prepared according to Rao *et al.* using dodecylamine as the amine template. X-Ray absorption spectroscopy was used to study changes in the Ti local coordination environment during formation of the mesoporous material—starting from the alkoxide precursor, followed by hydrolysis and condensation to form poorly crystallized anatase upon heat treatment. Neutral amine inhibits the formation of dimers prior to the hydrolysis reaction and gives rise to a more connected local structure. The Ti site is highly distorted, with a coordination environment ranging between O_h and D_{4h} symmetry. A higher surface area (up to 260 $m^2\ g^{-1}$) results when acid washing is employed to remove the surfactant template, whereas a surface area of only 80 $m^2\ g^{-1}$ is obtained when the template is removed by heat treatment. Li insertion proceeds *via* a pseudo-capacitive behavior in the presence of dodecylamine (DDA), whereas an anodic peak at 1.8 V *vs.* Li is present when the framework is condensed to form anatase. The incorporation of niobium atoms reinforces the structure, and the electrochemical behavior is more stable in cycling.

Introduction

Since the first mesoporous silicon oxides were reported in 1991 by researchers at Mobil,[1–7] extending this approach to transition metal oxides has been inhibited by difficulties in preparing template-free mesoporous metal oxides analogous to silica.[8–10]

For applications such as heterogeneous catalysis or photocatalysis, Ti atoms have been incorporated into the silica framework, either by an ion implantation method,[11] or by grafting of an organometallic complex on the surface.[12–15] More recently, a mesoporous titanosilicate (Ti-HMS) was prepared directly by the incorporation of Ti atoms into the MCM-41 framework.[16,17] Template titanium tetrabutoxide displacement has also been used.[18] Shrinkage of the pore diameter is generally observed for high Ti loading.[19] A mixed xerogel of composition $(TiO_2)_x(SiO_2)_{1-x}$ has been prepared by the hydrolysis of tetraethyl orthosilicate in the presence of titanium isopropoxide.[20]

For Ti-rich compositions, silica-free mesoporous TiO_2 can be prepared in the absence of a silica support. This may have application in dye-sensitized solar cells,[21] in fuel cells as a porous exchange membrane for proton conductivity,[22] or as a Li-ion negative electrode.[23] Various syntheses of TiO_2 mesoporous materials have been reported, including examples using a modified "sol–gel" process involving titanium isopropoxide bis(acetylacetonate) and alkylphosphate surfactants.[10] Ideally, removal of the surfactant from the materials would leave a very large porous structure, in which the pore size distribution is related to the size and arrangement of the surfactant within the material. Unfortunately, complete surfactant removal from these structures without collapse of the framework is difficult; often it is found that the surfactant acts as stabilizing species and cannot be fully extracted. In mesoporous TiO_2 formed with alkylphosphate surfactants, for example, there is substantial incorporation of the phosphate head groups into the wall structure after surfactant "removal". X-Ray diffraction and transmission electron microscopy observations suggest a meso-lamellar structure is actually achieved in these materials, not a strictly mesoporous structure.[24]

To decrease any attractive strength between the surfactant and the inorganic framework, and, to some extent, decrease the organic residue content in the final mesoporous material, neutral surfactants such as dodecylamine (DDA) and hexadecylamine (HDA) are required.[8,9,25] Other structure-directing agent may be used, such as β-cyclodextrin with urea,[26] or D-glucose.[27] Low concentrations of these specially shaped templates are sufficient to obtain mesoporous phases, but they give rise to highly disordered pore structures. Well-defined mesoporous TiO_2 spheres can be prepared *via* slow hydrolysis of $Ti(OPr)_4$ with DDA.[28] Alternatively, dispersed nanosized titania particles may be prepared by other methods, such as electrodeposition,[29] infiltration through a 3D template,[30] or thin-film methods.[23]

When Ti atoms are anchored to silica walls, they exhibit T_d symmetry,[11,31] whereas highly distorted Ti–O sites (mostly O_h) are observed for Ti incorporated in HMS walls.[16] To our knowledge, no study has been performed to characterize the intimate nature of mesoporous titania. A recent report describes the thermal behavior of titania formed using hexadecyltrimethylammonium bromide (CTAB) as the template.[32] It is found that the titania walls are destroyed at 400 °C. Here, we use DDA as the pore-forming agent and employ X-ray absorption spectroscopy to understand how the collapse of the 3D mesostructure occurs at each step. This picture differs from the recently reported non-assisted surfactant pathway,[33] as will be shown.

†Basis of a presentation given at Materials Discussion No. 5, 22–25 September 2002, Madrid, Spain.

Titanium oxides also have been extensively studied as potential candidates for negative electrode materials in Li-ion batteries.[34–39] Both TiO_2 and the lithium-deficient titanium spinel $Li_4Ti_5O_4$ have been studied. Compared to graphite,[40] titania is a low strain battery material that fulfills safety requirements, at the expense of exhibiting a higher discharge potential.[41] Moreover, titania is readily available, cheap, and nontoxic. Large diffusion pathways and the high surface area provided by a mesostructure may be an advantage for Li diffusion, especially as electrolyte can permeate the interior of the mesopores. Here, the Li insertion process is studied as a function of DDA removal, *viz*. surface area, *via* heat treatment or acid washing. The electrochemical behavior is compared to commercially available high surface area titania. Finally, niobium atoms are introduced in the titania walls to reinforce the structure. Electrochemical results are reported as a function of Nb loading.

Experimental

Synthesis of mesostructured titania

In a typical preparation, dodecylamine (DDA; 98%, Aldrich; 1.12 g, 6 mmol) was dissolved in 2-propanol (PrOH; reagent grade; 12.02 g, 200 mmol) and titanium isopropoxide [$Ti(OPr^i)_4$; 99.999%, Aldrich; 5.70 g, 20 mmol] was then added to the mixture. After 15 min, deionized water (10.81 g, 60 mmol) was slowly added. The hydrolysis product mixture was covered and aged at room temperature for 18 h. The resulting white precipitate was filtered off, rinsed with water and ethanol, and dried at 110 °C for 6 h. In order to prepare the Nb–Ti oxides, niobium ethoxide was added to the titanium isopropoxide before the hydrolysis reaction, in Nb/Ti proportions ranging from 10 to 25%.

Surfactant removal

Thermal treatment is often employed to remove surfactant from mesostructured metal oxides, but in the case of TiO_2 materials, this often results in collapse of the framework. A leaching process to extract the amine is preferable. To achieve this, the mesostructured, template-containing material was dispersed in a 50 : 50 ethanol–water mixture, to which different concentrations of HCl (10 to 50 mM) were added. Following a short reaction time, the material was filtered off and dried as before. The amount of residual surfactant was quantified by elemental analysis. Experimentally, we found that up to 50% of the initial surfactant content is removed when the sample is stirred with 20 mM HCl for 30 min.

Ti-HMS

This material was prepared according to literature reports[16] by using DDA as the neutral surfactant and ethanol as the co-solvent. A solution of tetraethyl orthosilicate (TEOS) and titanium isopropoxide (Ti/Si molar ratio of *ca.* 2%) was added to a vigorously stirred DDA–EtOH mixture, and the resultant solid was filtered off and treated as above.

Commercial titania

Bulk anatase (99.9+%, Aldrich), nanocrystalline anatase (Hombikat UV 100®, Sachtleben Chemie) and mesostructured titania (Mesotech Modern Materials) were used as received.

Instrumentation

Powder X-ray diffraction (XRD) analysis was performed on a Siemens D500 X-ray diffractometer with a diffracted beam monochromator and Cu-Kα source. Thermal gravimetric analysis (TGA) and differential thermal analysis (DTA) were performed simultaneously on a PL Thermal Sciences STA 1500 thermal analysis system. Brunauer–Emmett–Teller (BET) specific surface areas of the mesostructured samples were determined by nitrogen adsorption techniques, using a Quantachrome Autosorb-1 instrument.

X-Ray absorption spectroscopy

Experiments were performed at the LURE facility (Orsay, France) using X-ray synchrotron radiation emitted by the DCI storage ring at the D44 beam line. Spectra were collected at room temperature in the transmission mode. For EXAFS, a double-crystal Si(111) monochromator scanned the energy in 2 eV steps from 100 below to 900 eV above the Ti K-absorption edge (4966 eV). Three spectra were recorded for each sample, with an accumulation time of 2 s per point. The extracted $k\chi(k)$ spectra are displayed in Fig. 1. For XANES, a double-crystal Si(311) monochromator was used. Two spectra were recorded from 4950 to 5100 eV in steps of 0.25 eV, with 1 s of accumulation time per point. The analysis of the EXAFS data was performed as previously reported[42] using either the program package developed by A. Michalowicz[43] or WINXAS 97[44] using the amplitude and phase functions from Mac Kale or Feff tables, respectively. It is important to note that the two types of data treatment give very similar results. Special care was taken in considering the number of variable parameters. At the beginning of the procedure, for which only the Ti–O shell was considered, the Δk and ΔR ranges are 12.24 $Å^{-1}$ and 1.0 Å, respectively. In a second step, the other contributions of the radial distribution function (RDF) were considered, and the first Ti–O contribution was kept unchanged. In this case, ΔR = 2.1 Å. Fig. 2 allows the reader to visualize the quality of the fits. Rutile TiO_2 and Ti_2O_3 were used as reference materials.

Electrochemical studies

The active material was first passed through a 50 μm mesh and then mixed with acetylene black and polyvinylidene fluoride

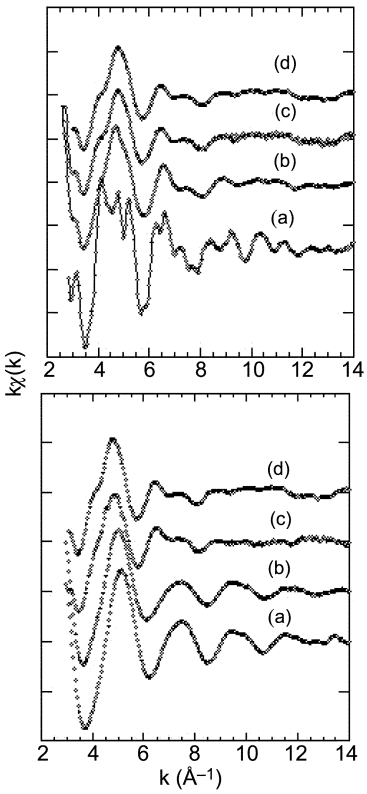

Fig. 1 Extracted EXAFS data for various samples. Above: (a) rutile; (b) 460 °C TiO_2; (c) solid obtained without DDA; (d) dried sample. Below: (a) liquid without DDA; (b) liquid with DDA; (c) gel-like sample; (d) dried sample.

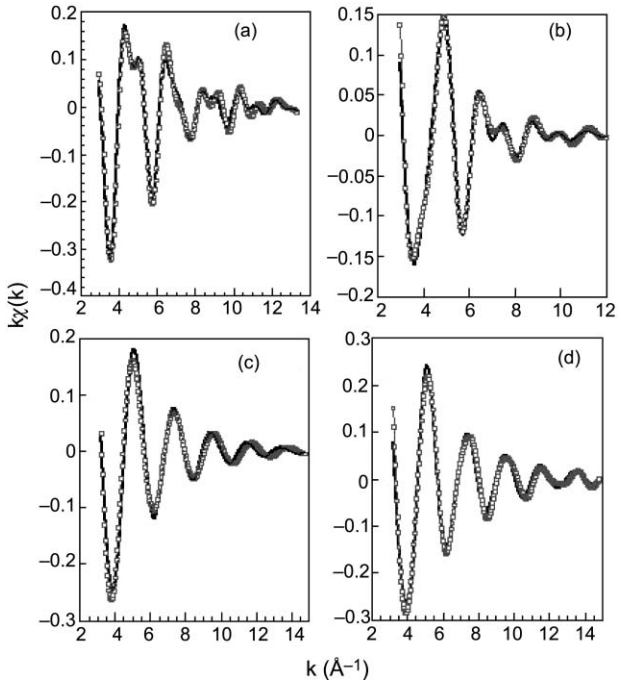

Fig. 2 Fitted EXAFS data for (a) rutile, (b) dried sample, (c) liquid with DDA, and (d) liquid without DDA. Points and lines represent experimental and theoretical values, respectively.

(PVDF) binder (80 : 15 : 5 m.w.) in cyclopentanone. The composite slurry was cast on a metallic nickel disc and air-dried. Typically, each composite electrode contained *ca.* 2 mg of active material. The reference and working electrode was lithium metal, and the electrolyte was 1.0 M $LiPF_6$ in EC/DMC (1 : 1 vol.). Swagelock-type cells were assembled in an argon-filled glove box. An electrolyte-soaked porous glass separator bridged the two electrodes, which were held in intimate contact through a spring-loaded system. The cells were cycled under ambient conditions on a multi-channeled galvanostatic/potentiostatic system (MacPile, France). Typically, current densities of 20 and 15 mA g^{-1} were used for the discharge and charge processes, respectively.

Results and discussion

From liquid to solid

The results of the EXAFS fit for rutile TiO_2 are in good agreement with the crystallographic data (Table 1). As a

Table 1 XAS fit results for reference samples. Crystallographic data are reported

Sample	Shell	*N*	*R*/Å	$\sigma^2/10^{-2}$ Å^2	Reference or ρ^a (%)
Rutile (lit.)	Ti–O	4	1.949		Ref. 45
	Ti–O	2	1.980		
	Ti–Ti	2	2.959		
Rutile (exp.)	Ti–O	6	1.96	0.57	
	Ti–Ti	2	2.96	0.94	2.0
Ti_2O_3 (lit.)	Ti–O	3	2.012		Ref. 46
	Ti–O	3	2.083		
	Ti–Ti	1	2.590		
	Ti–Ti	4	2.989		
Ti_2O_3 (exp.)	Ti–O	6	2.05	0.55	
	Ti–Ti	1	2.59	0.58	
	Ti–Ti	4	2.99	1.46	2.4

$^a\rho = [\Sigma\{k^3\chi_{exp}(k) - k^3\chi_{theo}(k)\}^2/\Sigma\{k^3\chi_{exp}(k)\}^2]^{1/2}$. The commonly accepted fitting accuracy is about 0.02 Å for distance and 15 to 20% for the number of neighbors.

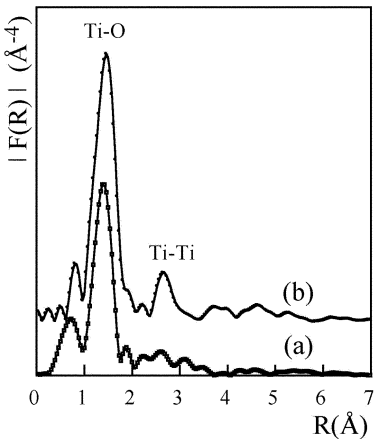

Fig. 3 FT moduli of $Ti(OPr^i)_4$ (a) with DDA and (b) without DDA. Distances are not corrected for phase shift.

further check of the validity of the data treatment, the same protocol was also used to successfully refine the Ti local order in Ti_2O_3.

Ti environment prior to hydrolysis. The local Ti environment in $Ti(OPr^i)_4$ was studied and compared to that obtained after placing the compound in an Pr^iOH solution with or without DDA. Fig. 3 shows the moduli of the Fourier transform corresponding to a pseudo-radial distribution function around the Ti atoms. The first intense peak attributed to the Ti–O contribution is best fit with 4 oxygen atoms. The Ti–O distance is in agreement[47] with the presence of Ti^{IV} (Table 2). In the absence of DDA, an additional shell arising from a light backscatterer needs to be added to improve the goodness of fit. The additional distance may contribute to a very small valency effect if the contribution is assigned to oxygen atoms ($\approx$ 0.2 valency units).

We could find no evidence of a contribution at longer distances for Ti alkoxide–DDA mixtures, whereas an additional peak is observed when Pr^iOH is added to the alkoxide. This peak is fit as a contribution from Ti–Ti atoms (Table 2). Our finding differs from previous results,[48] where a Ti–Ti correlation was found for $Ti(OEt)_4$ and $Ti(OBu)_4$ alkoxides, but an oligomeric assembly was not evident for $Ti(OPr^i)_4$. Additionally, it was claimed that a short Ti–O distance of 1.76 Å is combined with a coordination of three. We have no explanation for such a discrepancy. If we surmise that $Ti(OPr^i)_4$ entities remain isolated, the FT moduli should be superimposable. It has also been found that the hydrolysis of acetylacetonate-modified Ti alkoxides leads to the formation of dimers in which six-fold coordinated Ti atoms share edges through oxo-bridges.[49] Considering two $Ti(OPr^i)_4$ molecules 3.02 Å apart and rotated 90° from each other as shown in Fig. 4, the distance from a metal atom to an oxygen atom of the adjacent molecule is close to that obtained by EXAFS refinement, although the calculated coordination number is underestimated.

The fact that DDA appears to suppress the contribution from Ti–Ti correlations suggests that condensation or dimerization does not occur in its presence. However, ^{15}N NMR data do not show evidence of a direct interaction between DDA and

Table 2 XAS fit results for $Ti(OPr^i)_4$ in Pr^iOH in the absence and presence of DDA

	Shell	*N*	*R*/Å	$\sigma^2/10^{-2}$ Å^2	ρ (%)
Without DDA	Ti–O	4.7	1.84	0.29	
	Ti–O	1	2.4	0.64	
	Ti–Ti	1.2	3.02	0.81	1.6
With DDA	Ti–O	4.5	1.84	0.53	1.3

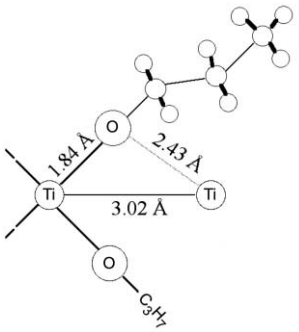

Fig. 4 Model for the $Ti(OPr^i)_4$ dimer.

$Ti(OPr^i)_4$.[25] DDA must weakly interact with Ti alkoxide entities, thus inhibiting association, and acting to disperse the Ti alkoxide and slow down hydrolysis. The mixing of the two prior to hydrolysis is, therefore, necessary to obtain a mesostructured framework.

Optimization of the synthesis

When the DDA/$Ti(OPr^i)_4$ solution is hydrolyzed, it turns white and a gel is immediately formed. Due to the electrophilic character of the metal, the reactivity of metal alkoxides is quite high for Ti compared to Si. Acetylacetonate (acac) is usually added to slow down the hydrolysis reaction. Even with acac addition, a gel is rapidly formed, although increasing the amount of acac induces a decrease in crystallinity, as shown in Fig. 5. The peak at 29 Å ($2\theta = 3.05°$) is characteristic of the mesostructured material that results from using DDA as the template.[25] The peak is assigned to the (001) reflection arising from a disordered hexagonal mesostructured arrangement of template/oxide precursor. The incorporation of acac decreases the observed XRD intensity, and a large amount almost completely suppresses the formation of crystalline product, giving rise to an amorphous sample [Fig. 5(c)].

We employed several different surfactants and Ti sources in the absence of acac to form the mesostructured products. The resultant XRD patterns are displayed in Fig. 6. Using $Ti(OPr^i)_4$ as a precursor, the surfactant DDA [Fig. 6(b)] gives rise to a more ordered material than decylamine, [Fig. 6(a)]. The peak is slightly shifted to a larger *d*-spacing when HAD is used as the

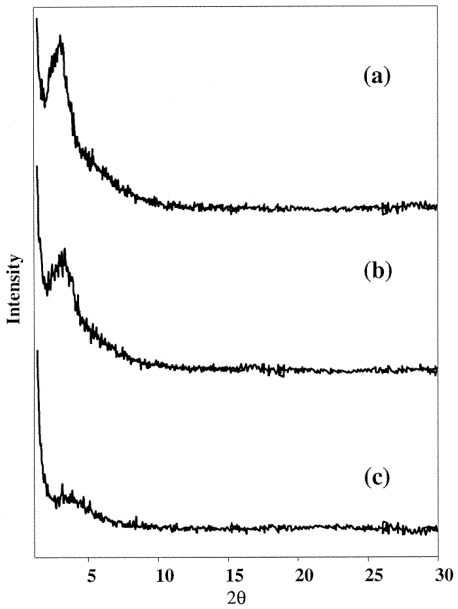

Fig. 5 XRD patterns of mesostructured titania prepared with acac to Ti alkoxide ratios of (a) 0.12 : 1, (b) 0.35 : 1, and (c) 0.98 : 1.

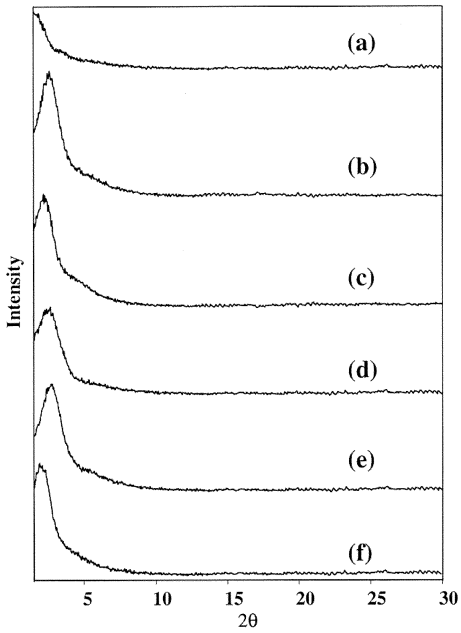

Fig. 6 XRD patterns of mesostructured titanias prepared from (a) decylamine and titanium isopropoxide, (b) dodecylamine and titanium isopropoxide, (c) hexadecylamine and titanium isopropoxide, (d) decylamine and titanium ethoxide, (e) dodecylamine and titanium ethoxide, and (f) hexadecylamine and titanium ethoxide.

template [Fig. 6(c)], in accord with the longer chain length of this surfactant. Comparison of Fig. 6(b) and (e) and Fig. 6(c) and (f) reveals that using titanium ethoxide or isopropoxide in the presence of the same neutral surfactant results in products with similar XRD patterns. The only exception occurs with titanium ethoxide–decylamine, which provides a more crystalline product [compare Fig. 6(d) to Fig. 6(a)]. Aging time and heat treatment temperature were also optimized in a similar manner. Diffraction peaks at higher angles are absent from these XRD patterns, suggesting a high level of disorder in the walls. To shed some light on the local order present in the framework, XAS measurements were performed.

Ti local order

Near edge absorption. The features in the absorption edge are sensitive to the immediate Ti environment. For the K edge, the existence of a pre-edge and its intensity are closely related to the degree of d–p orbital mixing and the departure from a centrosymmetric environment. The edge jump corresponds to the transition of electrons to bound excited electronic states. For example, in a tetrahedrally coordinated Ti atom [*i.e.* $Ti(OPr^i)_4$], the dipolar transition gives rise to an intense pre-edge feature [Fig. 7(a)]. More symmetric sites result in its decrease, as illustrated in the spectra of fresnoite[50] [Fig. 7(b)] and rutile [Fig. 7(c)], where Ti atoms are coordinated to oxygen to form a highly distorted square pyramid or an octahedral environment, respectively.

Previous XANES studies on several Ti^{IV}-containing minerals established a quantitative comparison between pre-edge intensity and energy with coordination number.[51–53] Our results confirm this trend, as higher coordination number clearly results in a higher pre-edge energy associated with a lower intensity (Fig. 7). The characteristics of the XANES spectrum for the mesostructured material [Fig. 7(d)] reveal that the Ti environment is at the border between coordination numbers 5 and 6. The pre-edge intensity is greater than that of rutile (Fig. 7, inset), although the three main spectral features present in rutile are observed. These have been attributed to 3d–4p and 4p–4s transitions, based on a multiple scattering model calculation.[54] Not surprisingly, this shows that near edge

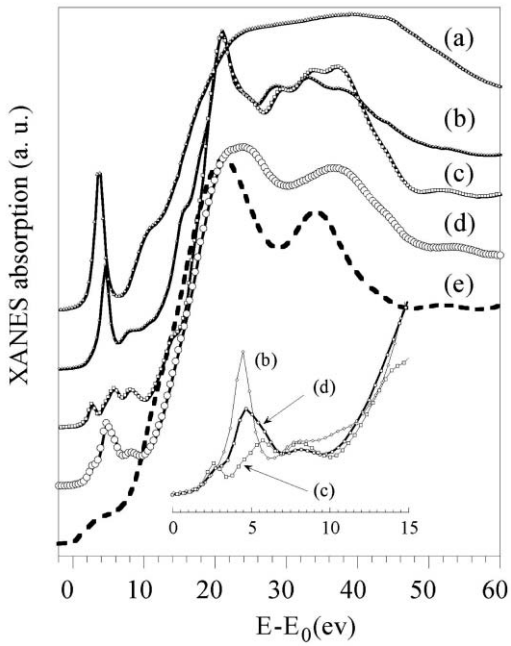

Fig. 7 XANES spectra of (a) $Ti(OPr^i)_4$, (b) fresnoite, (c) TiO_2 rutile, (d) mesostructured titania, and (e) Ti_2O_3. The absorption has been normalized at 5046 eV. E_0 is taken at the edge of Ti metal (4966.4 eV).

features are only sensitive to the nearest Ti–O neighbors, since the mesostructured phase most definitely differs from the condensed rutile phase at a longer length scale (*vide infra*). Note also that the combination of pre-edge and main edge shapes and positions allows us rule out the possibility of a mixture of Ti atoms in both 4- and 6-coordinate environments. Furthermore, if the pre-edge features were the result of superimposed rutile and $Ti(OPr^i)_4$ or fresnoite spectra, such a mixture would give a much more complex main edge containing at least two well-separated features. Such features are completely absent. Therefore the EXAFS spectra are fit assuming the presence of a unique Ti environment.

EXAFS study. The FT modulus of the mesostructured phase is displayed in Fig. 8. By comparison to the precursor $Ti(OPr^i)_4$ (Fig. 3), significant changes occur on hydrolysis as expected based on the modification of the coordination number and the Ti atom environment during the reaction. The first peak composed of overlapped contributions is fit with the three distinct Ti–O distances [Table 3 and Fig. 8(a)]. The distribution of Ti–O distances is consistent with a distorted site. This

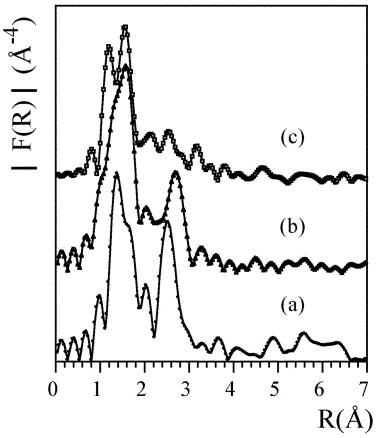

Fig. 8 FT modulus of (a) mesostructured titania, (b) no DDA-assisted material, and (c) commercial Mesotech TiO_2. Distances are not corrected for phase shift.

Table 3 XAS fit results for the materials after hydrolysis

	Shell	N	R/Å	$\sigma^2/10^{-2}$ Å^2	ρ (%)
With DDA	Ti–O	2.9	1.91	0.59[a]	
	Ti–O	2.4	2.06	0.59[a]	
	Ti–O	0.8	2.21	0.55	
	Ti–O[b]	0.5	2.4	0.25	
	Ti–Ti	2.3	3.08	1.21	1.2
Without DDA	Ti–O	3.8	1.92	0.72[a]	
	Ti–O	2.2	2.08	0.72[a]	
	Ti–O[b]	1.6	2.58	0.88	
	Ti–Ti	1.0	3.05	0.74	1.0
Mesotech	Ti–O	2.0	1.87	0.64[a]	
	Ti–O	2.7	2.00	0.64[a]	
	Ti–O[b]	1.0	2.66	0.36	
	Ti–Ti	1.2	3.16	1.44	
	Ti–Ti	3.9	3.87	2.25	1.5

[a]Debye–Waller factors were kept equal during the fitting procedure. [b]The nature of the backscattering atom is discussed in the text.

provides further evidence of a strong distortion of the Ti coordination polyhedra, leading to D_{3h} or C_{4v} symmetry. A Ti–Ti contribution is also present (Table 1), along with an additional contribution whose nature is puzzling and difficult to disentangle, as the Δk range is rather narrow (12.34 Å^{-1}). Possible assignments include nitrogen atoms capping the polyhedron, oxygen atoms completing the coordination, or a short Ti–Ti correlation. Two of these can be readily discounted. With respect to the first, we note that nitrogen–metal coordination has been observed in a range of compounds, including pyridine in a layered molybdenum oxide[55] and in silica–titania xerogels.[20] However, we see evidence of the additional contribution in our case in the absence of either DDA or acac (see below), and thus rule out this contribution. Considering a Ti atom as the backscatterer,[56] such a short Ti–Ti distance would necessarily correspond to face-sharing octahedra as present in reduced oxides such as Ti_2O_3. No shift is observed in the XANES spectra between the rutile and the mesostructured phase, however, whereas the spectrum of Ti_2O_3 is shifted by -2.20 eV, as expected [Fig. 7(e)].[57] This shows that the contribution is associated with oxygen atoms and, consequently, may explain the difficulty in assigning the coordination number as an integer value.

The presence of DDA influences the Ti local order (Table 3), as might be expected. The number of Ti–Ti correlations is smaller in the absence of the neutral surfactant [Fig. 8(b)], highlighting the role of DDA in establishing the framework connectivity. Without DDA, the oxygen environment exhibits a strong tendency toward C_{4v} symmetry. These results are different to those reported by Luca *et al.*[33] for an analogous material; they reported the presence of a T_d site and a short Ti–O distance of 1.85 Å. However, the presence of T_d titanium coordination was not supported by XANES.[33]

The pseudo-radial distribution function of commercial mesoporous TiO_2 from Mesotech is shown for comparison in Fig. 8(c).[25] This material exhibits a surface area of 630 m^2 g^{-1}, associated with an average pore size distribution of 32 Å. The XRD suggests somewhat poor ordering of the pores. The oxygen contribution may be described with two Ti–O distances, slightly smaller than in our mesostructured material (Table 3). The presence of Ti–Ti correlations indicates that, despite its featureless XRD pattern, the Mesotech sample has some long range order.

From the mesostructured TiO_2 phase to anatase

The mesostructured assembly is retained up to 260 °C, as shown in the XRD pattern (Fig. 9), although a decrease in crystallinity accompanies the process. Treatment at higher temperatures leads to the formation of TiO_2 (anatase). The corresponding thermal gravimetric/differential thermal curves

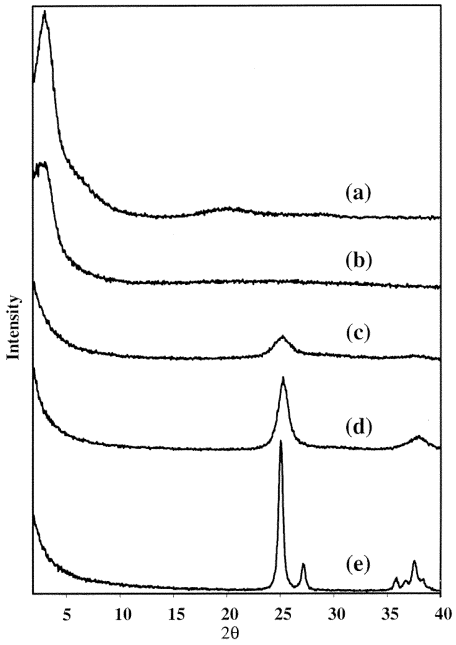

Fig. 9 XRD patterns of the mesostructured titania heat treated at (a) 25, (b) 260, (c) 460, (d) 515, and (e) 600 °C.

shown in Fig. 10 (recorded in air) are similar to those recently reported.[32] The first weight loss is attributable to adsorbed water and $Pr^{i}OH$. The exothermic process between 150 and 500 °C is attributed to the removal of DDA by combustion. The phenomenon at *ca.* 500 °C is attributed to oxidative combustion of the remaining DDA residues, concomitant with the formation of anatase.

Refinements of the EXAFS spectra of the heated samples were performed, and the fits are summarized in Fig. 11. The data shows that the oxygen environment is maintained up to a temperature of 320 °C, with octahedral symmetry being maintained at the Ti site. An additional long Ti–O distance that is apparent in materials treated below 320 °C disappears at higher temperature. This implies that the removal of DDA does not have a significant effect on the framework. In contrast, the Ti sites in titania/silica mixed xerogels change from O_h to T_d upon heat treatment.[20]

Electrochemical results

When the sample heated at 460 °C is cycled between 2.5 and 0.9 V *vs.* Li, the reversible capacity, Q_{rev}, is approximately 1/2

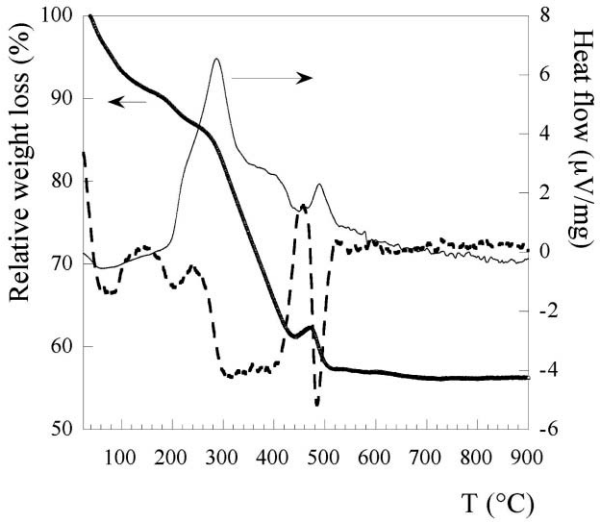

Fig. 10 TGA and DTA curves for the mesostructured titania.

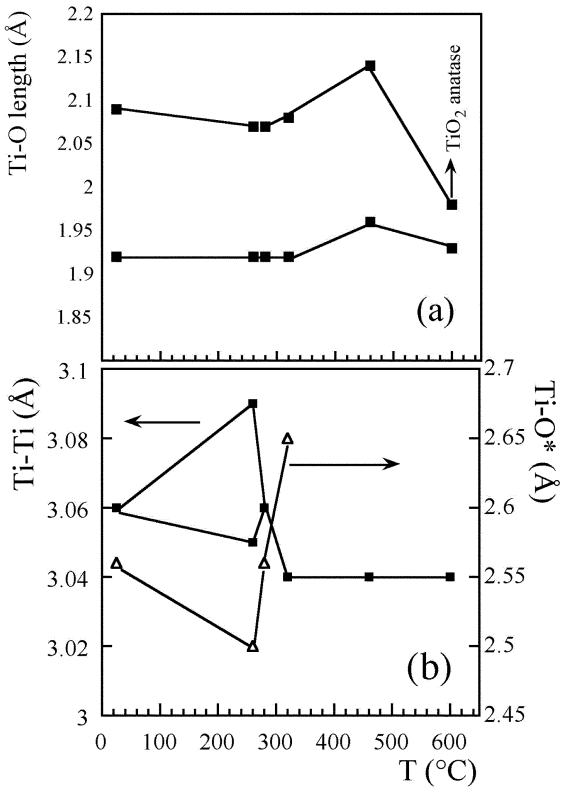

Fig. 11 Evolution of (a) Ti–O and (b) Ti–Ti and long Ti–O distances (see text) obtained from least-square fitting of the XAS signal. Data for anatase are taken from the literature.[58]

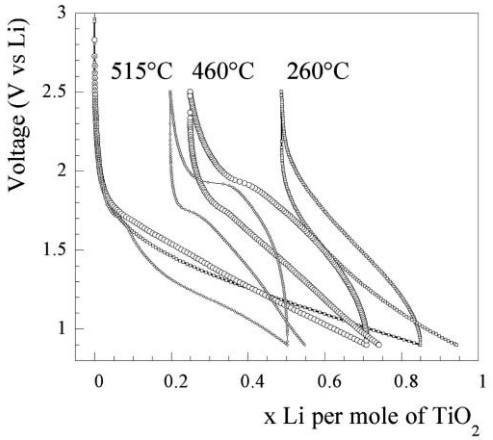

Fig. 12 Li insertion profiles for heat-treated samples. The heat treatment temperatures are indicated on the plots.

Li per mole of TiO_2, as shown in Fig. 12 (Q_{rev} is the capacity in the first charge). Q_{rev} is, however, associated with an irreversible response. This is due to Li ions being trapped in the material during the first discharge. For materials heat treated above or below 460 °C, the capacity is lower. Below 460 °C, DDA molecules remain in the pores, resulting in a large irreversibility (up to 60% of the total first discharge). At 515 °C, densification occurs, giving rise to a large polarization which is observed in the voltage–composition curves and acts to lower the observable capacity.

To obtain a clearer picture of the processes that occur during Li insertion/deinsertion, the electronic density curves (Fig. 13) were examined. A Li insertion site is observed at 1.75 V *vs.* Li, in accord with previous studies of TiO_2.[34] This reversible process appears on the second discharge for the sample treated at 460 °C. An additional discharge peak is observed at 1.2 V *vs.*

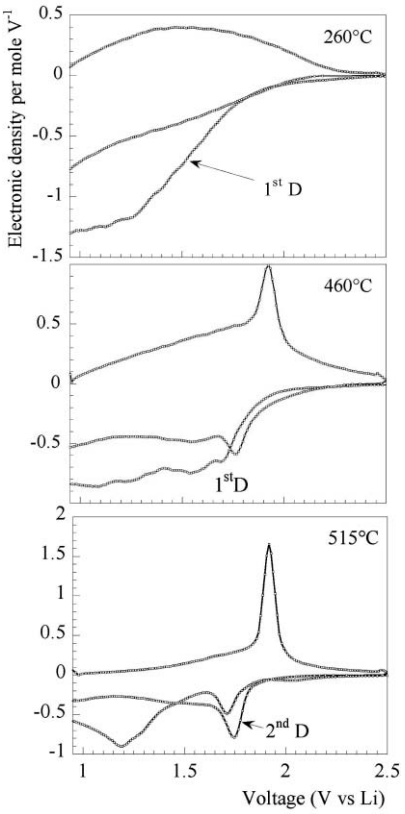

Fig. 13 Electronic density curves corresponding to Fig. 10.

Li (T = 515 °C), but a corresponding peak is not observed when charging, showing that this irreversible process may be the origin of the large polarization. After heat treatment of the mesostructured material at 260 °C, a featureless profile is observed, characteristic of multi-site insertion[59] or the pseudo-capacitive behavior[60] displayed by amorphous materials.[61] To further characterize Li insertion, the discharge cut-off potential was lowered. An intercalation of *ca.* 1 Li is reached for V_d = 5 mV, but is associated with a dramatic increase in the irreversibility.

The mesoporous materials in which the template was removed by acid washing differ in their response to electrochemical Li insertion. In these materials, the hexagonal mesostructural order is maintained on extraction of up to 50% of the DDA from the sample. The surface area increases from 15 to 220 m^2 g^{-1} after template removal. Li insertion results in a reversible capacity close to that obtained for the 460 °C heat-treated sample, but the irreversible contribution is doubled. Thus, the open structure may be beneficial for Li insertion, but it also has the drawback of irreversible reactions as a result of high surface area (and residual reactive surface groups). Li-ion uptake is proportional to DDA removal. In the total absence of DDA during the synthesis, the reversible capacity corresponds to 0.65 Li/Ti, but it rapidly falls upon cycling. The Mesotech mesoporous TiO_2 exhibits a low Li insertion capacity associated with a large irreversibility.

Highly crystalline anatase exhibits a small Li insertion capacity (0.1 Li/Ti), associated with a tremendous polarization. The voltage profile for the Hombikat UV 100 resembles that of the 515 °C heat-treated titania (Fig. 14). Similarly, a pronounced plateau at 1.8 V is observed under discharge, accompanied with a small polarization. The cyclability of Hombikat UV 100 is poor. This arises from the low voltage portion, as exemplified in Fig. 14(b). By using a cut-off voltage of 1.5 V, the capacity is maintained for a few cycles.

The effect of the interface on the electrochemical behavior was examined for the different materials. A measure of the

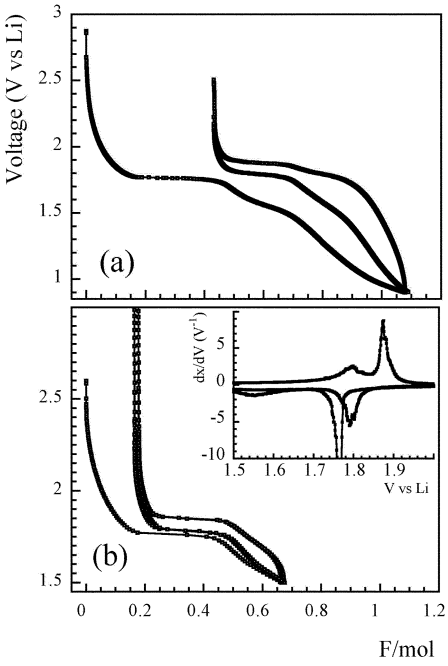

Fig. 14 Voltage profile for Hombikat UV 100 in the voltage ranges (a) 2.5–0.9 V *vs.* Li and (b) 3.0–1.5 V *vs.* Li, with dx/dV *vs.* V curves displayed in the inset.

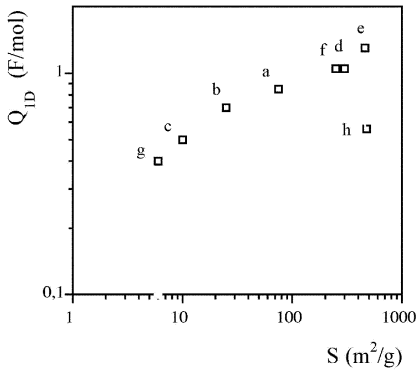

Fig. 15 Q_{1D} *vs.* surface area for several titania materials: Mesostructured samples heat treated at (a) 260, (b) 460, and (c) 515, (d) mesoporous titania obtained by acid washing, (e) non DDA-assisted TiO_2, (f) Hombikat UV 100 TiO_2, (g) anatase (Aldrich), and (h) Mesotech TiO_2. The voltage domain is 2.5–0.9 V *vs.* Li.

interface is taken as the surface area, S. In a log–log representation, the total first discharge capacity is found to be dependent on S (Fig. 15). On the other hand, the irreversible portion is not proportional to S. This shows that some irreversible events are not only due to interface effects, but also to irreversible trapping of Li ions. Particle size is of importance as well. In spite of a high surface area, the Mesotech material performance is similar to anatase, and lower than the other materials. The Mesotech sample has an average particle size of 150 nm, whereas our sample treated at 515 °C and Hombikat UV 100 exhibit a particle size of less than 10 nm.

Ti, Nb mixed mesostructured oxides

Niobium cations have been incorporated in the titania framework to stabilize the structure.[62] The samples have similar X-ray patterns to the niobium-free materials. Our EXAFS study shows that two Ti–O distances are present at 1.92 and 1.98 Å, slightly shorter than for the Nb-free sample. The Ti site remains unchanged for a Nb^{IV} concentration of up to 25 wt.% The inclusion of Nb atoms improves the reversibility of the

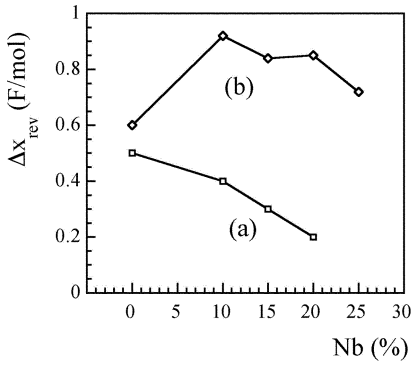

Fig. 16 Reversible capacity as a function of Nb atom doping for a voltage cut-off *vs*. Li of (a) 1.5 V and (b) 0.5 V.

Li insertion process, and also the reversible capacity. This is dependent on the voltage cut-off, as shown in Fig. 16. An optimum value is reached for 10 wt% Nb^{IV} associated with a cut-off voltage of 0.5 V *vs*. Li. For a higher cut-off voltage of 1.5 V, Nb incorporation decreases the reversible capacity. The voltage profile is characteristic of a multi-site insertion process.

Conclusion

The formation of a mesostructured titania using a neutral surfactant can be characterized from a local order point of view. We find that DDA molecules inhibit the dimerization of $Ti(OPr^i)_4$ at the start. On hydrolysis, the environment surrounding the Ti atom changes from T_d to highly distorted O_h. The presence of the surfactant, DDA, leads to a metal oxide framework that displays a greater degree of condensation or order, as shown by the greater number of Ti–Ti correlations. Partial loss of the surfactant by heat treatment at 260 °C increases the surface area from 25 to 80 $m^2\ g^{-1}$. The porous framework collapses at higher temperatures, giving rise to the formation of anatase. A larger surface area of 260 $m^2\ g^{-1}$ can be accessed by using acid washing to remove the surfactant from the pores.

Li insertion in the mesostructured materials proceeds *via* multi-site filling, a characteristic of the amorphous nature of the walls, in materials heat treated up to a temperature of 460 °C. The performance in terms of storage and release of the Li ions is hampered by the presence of DDA, however. With complete departure of DDA, the sample performs as well as Hombikat UV 100, a high surface area crystalline anatase, with a capacity of 155 mA h g^{-1} in the 2.5 to 0.9 V *vs*. Li voltage domain.

Acknowledgements

Financial support for this research was provided by NSERC through the strategic program (L. F. N.). The authors thank Dr Valérie Briois (LURE) for her help in acquiring the XANES and EXAFS data. We acknowledge the experimental opportunities at LURE (Orsay, France) supported by the CNRS.

References and notes

1 C. T. Kresge, M. E. Leonowicz, W. J. Roth, J. C. Vartuli and J. S. Beck, *Nature*, 1992, **395**, 710.
2 J. S. Beck, J. C. Vartuli, W. J. Roth, M. E. Leonowicz, C. T. Kresge, K. D. Schmitt, C. T.-W. Chu, D. H. Olson, E. W. Sheppard, S. B. McCuller, J. B. Higgins and J. L. Schlenker, *J. Am. Chem. Soc.*, 1992, **114**, 10834.
3 S. B. McCullen, J. C. Vartuli, C. T. Kresge, W. J. Roth, J. S. Beck, K. D. Schmitt, M. E. Leonowicz, J. L. Schlenker, S. S. Shih and J. D. Lutner, in *Access in Nanoporous Materials*, ed. T. J. Pinnavaia and M. F. Thorpe, Plenum Press, New York, 1995, p. 1.
4 P. T. Tanev and T. J. Pinnavaia, *Science*, 1995, **267**, 865.
5 D. M. Antonelli and J. Y. Ying, *Chem. Mater.*, 1996, **8**, 874.
6 P. Liu, I. L. Moudrakovski, J. Liu and A. Sayari, *Chem. Mater.*, 1997, **9**, 2513.
7 D. M. Antonelli, A. Nakahira and J. Y. Ying, *Inorg. Chem.*, 1996, **35**, 3126.
8 N. Ulagappan and C. N. R. Rao, *Chem. Commun.*, 1996, 1685.
9 N. Ulagappan, N. Battaram, V. N. Raju and C. N. R. Rao, *Chem. Commun.*, 1996, 2243.
10 D. M. Antonelli and J. Y. Ying, *Angew. Chem., Int. Ed. Engl.*, 1995, **34**, 2014.
11 T. Maschmeyer, F. Rey, G. Sankar and J. M. Thomas, *Nature*, 1995, **378**, 159.
12 Z. Zhang, C.-C. Wang, R. Zakaria and J. Y. Ying, *J. Phys. Chem. B*, 1998, **102**, 10871.
13 H. Yamashita, M. Honda, M. Harada, Y. Ichihashi, M. Anpo, T. Hirao, N. Itoh and N. Iwamoto, *J. Phys. Chem. B*, 1998, **102**, 10707.
14 S. Ito, T. Deguchi, K. Imai, M. Iwasaki and H. Tada, *Electrochem. Solid State Lett.*, 1999, **2**, 34.
15 Y. Matsumoto, Y. Ishikawa, M. Nishida and S. Ii, *J. Phys. Chem. B*, 2000, **104**, 4204.
16 W. Zhang, M. Fröba, J. Wang, P. T. Tanev, J. Wong and T. J. Pinnavaia, *J. Am. Chem. Soc.*, 1996, **118**, 9164.
17 S. Zheng, L. Gao, Q.-H. Zhang and J.-K. Guo, *J. Mater. Chem.*, 2000, **10**, 723.
18 Z.-L. Hua, J.-L. Shi, L.-X. Zhang, M.-L. Ruan and X.-G. Zhao, *J. Mater. Chem.*, 2001, **11**, 3130.
19 M. S. Morey, S. O'Brien, S. Schwarz and G. D. Stucky, *Chem. Mater.*, 2000, **12**, 898.
20 D. M. Pickup, G. Mountjoy, G. W. Wallidge, R. Anderson, J. M. Cole, R. J. Newport and M. E. Smith, *J. Mater. Chem.*, 1999, **9**, 1299.
21 Y.-Q. Wang, S.-G. Chen, X.-H. Tang, O. Palchik, A. Zaban, Y. Koltypin and A. Gedanken, *J. Mater. Chem.*, 2001, **11**, 521.
22 F. M. Vichi, M. I. Tejedor-Tejedor and M. A. Anderson, *Chem. Mater.*, 2000, **12**, 1762.
23 L. Kavan, J. Rathousky, M. Grätzel, V. Shklover and A. Zukal, *Microporous Mesoporous Mater.*, 2001, **44–45**, 653.
24 R. L. Putnam, N. Nakagawa, K. M. McGrath, N. Yao, I. A. Aksay, S. M. Gruner and A. Navrotsky, *Chem. Mater.*, 1997, **9**, 2690.
25 D. M. Antonelli, *Microporous Mesoporous Mater.*, 1999, **30**, 315.
26 J.-Y. Zheng, J.-B. Pang, K.-Y. Qiu and Y. Wei, *J. Mater. Chem.*, 2001, **11**, 3367.
27 Y. Wei, D. Jin, T. Ding, W. H. Shih, X. H. Liu, S. Z. D. Cheng and Q. Fu, *Adv. Mater.*, 1998, **3**, 313.
28 L. Wang, S. Tomura, M. Maeda, F. Ohashi, K. Inukai and M. Suzuki, *Chem. Lett.*, 2000, 1414.
29 Y. Matsumoto, Y. Ishikawa, M. Nishida and S. Ii, *J. Phys. Chem. B*, 2000, **104**, 4204.
30 Q.-B. Meng, C.-H. Fu, Y. Einaga, Z.-Z. Gu, A. Fujishima and O. Sato, *Chem. Mater.*, 2002, **14**, 83.
31 M. D. Alba, Z. Luan and J. Klinowski, *J. Phys. Chem.*, 1996, **100**, 2178.
32 G. J. de A. A. Soler-Illia, A. Louis and C. Sanchez, *Chem. Mater.*, 2002, **14**, 750.
33 V. Luca, S. Djajanti and R. F. Howe, *J. Phys. Chem. B*, 1998, **102**, 10650.
34 S. Y. Huang, L. Kavan, I. Exnar and M. Grätzel, *J. Electrochem. Soc.*, 1995, **142**, L142.
35 B. Zachau-Christiansen, K. West, T. Jacobsen and S. Atlung, *Solid State Ionics*, 1988, **28–30**, 1176.
36 S. Bach, J.-P. Pereira-Ramos and N. Baffier, *J. Mater. Chem.*, 1998, **8**, 251.
37 M. E. Arroyo y de Dompablo, E. Moran, A. Varez and F. Garcia-Alvarado, *Mater. Res. Bull.*, 1997, **32**, 993.
38 B. O'Regan, J. Moser, M. Anderson and M. Grätzel, *J. Phys. Chem.*, 1990, **94**, 8720.
39 S. Y. Huang, L. Kavan, A. Kay and M. Grätzel, *Act. Pass. Elec. Comp.*, 1995, **18**, 23.
40 J. R. Dahn, A. K. Sleigh, H. Shi, B. M. Way, W. J. Weydanz, J. N. Reimers, Q. Zhong and U. von Sacken, in *Lithium Batteries, New Materials, Developments and Perspectives*, ed. G. Pistoia, Industrial Chemistry Library, vol. 5, Elsevier Science B.V., Amsterdam, 1994, p. 65.
41 K. Zaghib, M. Armand and M. Gauthier, *J. Electrochem. Soc.*, 1998, **145**, 3135.
42 F. Leroux, M. Adachi-Pagano, M. Intissar, S. Chauvière, C. Forano and J.-P. Besse, *J. Mater. Chem.*, 2001, **11**, 105.
43 A. Michalowicz, in *Logiciel Pour La Chimie*, Société Française de

Chimie, Paris, 1991, p. 102; available on the LURE website: http://www.lure.fr.
44 T. Ressler, *J. Phys. IV*, 1997, **7**, C2–269.
45 S. C. Abrahams and J. L. Bernstein, *J. Chem. Phys.*, 1971, **55**, 3206.
46 C. E. Rice and W. R. Robinson, *J. Solid State Chem.*, 1977, **21**, 145.
47 I. D. Brown and R. D. Shannon, *Acta Crystallogr., Sect. A*, 1973, **29**, 266.
48 F. Babonneau, S. Doeuff, A. Leaustic, C. Sanchez, C. Cartier and M. Verdaguer, *Inorg. Chem.*, 1988, **27**, 3166.
49 G. D. Smith, C. N. Caughlan and J. A. Campbell, *Inorg. Chem.*, 1972, **11**, 2989.
50 Ti–O distances in $Ba_2TiGe_2O_8$: 1 at 1.717, 2 at 1.923, and 2 at 1.965 Å, according to: R. Masse, J. C. Grenier and A. Durif, *Bull. Soc. Fr. Mineral.*, 1967, **90**, 20.
51 F. Farges, *Am. Mineral.*, 1997, **82**, 44.
52 F. Farges, *J. Non-Cryst. Solids*, 1996, **204**, 53.
53 G. A. Waychunas, *Am. Mineral.*, 1987, **72**, 89.
54 Z. Y. Wu, G. Ouvrard, P. Gressier and C. R. Natoli, *Phys. Rev. B*, 1997, **55**, 10382.
55 J. W. Johnson, A. J. Jacobson, S. M. Rich and J. F. Brody, *J. Am. Chem. Soc.*, 1981, **103**, 5246.
56 A. G. McKale, B. W. Veal, A. P. Paulikas, S.-K. Chan and J. Knapp, *J. Am. Chem. Soc.*, 1988, **110**, 3763.
57 J. Wong, F. W. Lytle, R. P. Messmer and D. H. Maylotte, *Phys. Rev. B*, 1984, **30**, 5596.
58 Distances in TiO_2 anatase: (O) 4 at 1.933 and 2 at 1.979 Å; (Ti) 4 at 3.0392 Å, according to: C. J. Howard, T. M. Sabine and F. Dickson, *Acta Crystallogr., Sect. B*, 1991, **47**, 462.
59 E. Schmidt, G. Meunier and A. Levasseur, *Solid State Ionics*, 1995, **76**, 243.
60 B. E. Conway, *J. Electrochem. Soc.*, 1991, **138**, 1539.
61 F. Leroux, Y. Piffard, G. Ouvrard, J.-L. Mansot and D. Guyomard, *Chem. Mater.*, 1999, **11**, 2948.
62 C.-C. Wang and J. Y. Ying, *Chem. Mater.*, 1999, **11**, 3113.